



Generation of Projector Augmented-Wave atomic data: A 71 element validated table in the XML format



François Jollet^{a,*}, Marc Torrent^a, Natalie Holzwarth^b

^a CEA, DAM, DIF, F-91297 Arpajon, France

^b Department of Physics, Wake Forest University, Winston-Salem, NC 27109, USA

ARTICLE INFO

Article history:

Received 30 September 2013

Received in revised form

26 November 2013

Accepted 25 December 2013

Available online 2 January 2014

Keywords:

PAW atomic data

ATOMPAW

ABINIT

ABSTRACT

In the Projector Augmented Wave (PAW) method developed by Blöchl (1994), a PAW data file is needed for each element, taking the role of the pseudopotential file used with the norm-conserving or ultrasoft formalisms. In this paper, we review methods for generating PAW data files and for evaluating their accuracy, transferability, and numerical efficiency in simulations of bulk solids. We have developed a new set of PAW atomic data files for most of the stable elements in the periodic table. These files are provided in a standard XML format for use in any PAW electronic structure code. The new dataset performs well as measured by the “ Δ ” evaluation criterion introduced by Lejaeghere et al. (2014), and also performs well in a modified evaluation scheme proposed in the present paper.

© 2014 Elsevier B.V. All rights reserved.

1. Introduction

In the context of Density Functional Theory (DFT) electronic structure calculations performed in the framework of the plane wave pseudopotential approach, the interaction between valence electrons and the ions formed by the atomic nucleus and the core electrons can be represented by an effective interaction known as a pseudopotential. The pseudopotential must be constructed for each element to represent the valence electron interactions in simulations of a wide variety of materials. During the past 30 years, much effort has been devoted to improving the accuracy, transferability, and efficiency of pseudopotential formulations. In 1979, Hamann, Schlüter, and Chiang [1] introduced the notion of norm-conserving (NC) pseudopotentials. A large number of numerical schemes have been proposed to construct NC pseudopotentials such as described in Refs. [2–4]. In this context, the pseudopotential files contain pseudo wavefunctions and corresponding pseudopotentials for each relevant quantum number “ l ”.

In order to decrease the number of plane waves required for the numerical convergence of DFT calculations in the NC pseudopotential framework, Vanderbilt introduced the concept of an ultrasoft (US) pseudopotential, for which the norm-conserving condition has been relaxed [5]. In addition, Blöchl [6] proposed a new formalism called the projector augmented wave (PAW) method which shares some of the plane wave convergence benefits

of the US scheme. Both the US and PAW formalisms use the notion of atomic projector functions that must be given in the pseudopotential file. The PAW method is based on a linear transformation between the all-electron (AE) and corresponding pseudo (PS) wavefunctions of an electronic state, together with the use of atom-centered AE and PS partial waves and their associated projectors. This PAW transformation ensures that the formalism is directly derived from the all-electron equations with well-controlled approximations. It can be shown that the US and NC formalisms can be derived from the PAW formalism [7] with the use of additional approximations.

The PAW formalism as developed by Blöchl [6] needs a “PAW atomic data” file for each element considered in the simulation. This data file includes both AE and PS partial wave basis functions and their corresponding projector functions together with additional information such as the local pseudopotential and the compensation charge parameters. Within the PAW formalism, there are a number of alternative implementations. For example, the construction of the PS basis and projector functions can be based on the method proposed in the original paper by Blöchl’s [6], or based on the compatible scheme developed by Vanderbilt in the formulation of the US method [8] (called here Vanderbilt’s scheme), or based on the RRKJ pseudization scheme [9] originally developed for NC pseudopotentials [10]. The PAW method has been implemented in several codes (see for instance [6,11,7,12–15]).

Within these PAW codes, there are additional variations in some of the details of the implementations. For example, in the Vienna ab initio simulation package (VASP) [12] the PAW treatment is based on the Kresse–Joubert formulation [7] which differs from

* Corresponding author.

E-mail address: francois.jollet@cea.fr (F. Jollet).

the original Blöchl formulation [6] in the treatment of the exchange–correlation contributions [16].

In addition to the large diversity of numerical formulations of the PAW method, it is sometimes necessary to adjust the method on the basis of the physical properties of the simulation system. For example, in the treatment of materials at high pressure, it can be necessary to include both semi-core and valence electron states in the PAW basis and projector set and to use small augmentation radii. In general, it is sometimes necessary to develop specialized PAW atomic data. With all of these competing considerations, it is clear that it is not possible to find a standardized PAW atomic data set that can meet all of the requirements of materials simulations. However, since reliable PAW atomic data are essential for realistic materials simulations, it is important to invest effort in their development and evaluation.

In this paper we review many different schemes for generating PAW atomic data and introduce a new PAW atomic dataset for 71 elements. We also discuss various evaluation criteria for the datasets in terms of accuracy, transferability, and computational efficiency. The paper is organized as follows. Section 2 presents the general background and formalism and summarizes several different schemes for generating the components of the PAW atomic data. Section 3 gives the methodology we have followed to generate a new PAW atomic dataset for 71 elements. Section 4 discusses validation and efficiency criteria for the atomic data. For validation, we use the Δ measure introduced by Lejaeghere et al. [17] and also introduce a modified criterion. These criteria are used to compare our new PAW atomic dataset with two other packages from the recent literature [18,19].

2. General background and formalism

The details of the PAW method have already been given several times in the literature [6,20,7].

In this paper, we use atomic units and adopt the notation of Ref. [7] and also use the specific formalism used in the ABINIT code [14] as described in Ref. [21].

The PAW method is based on a linear transformation linking the AE (all electron) wavefunctions Ψ_{nk} to the corresponding PS (pseudo) wavefunctions $\tilde{\Psi}_{nk}$. Here, the indices n and k refer to the band and wavevector indices, respectively.

$$|\Psi_{nk}\rangle = |\tilde{\Psi}_{nk}\rangle + \sum_i (|\phi_i\rangle - |\tilde{\phi}_i\rangle) \langle \tilde{p}_i | \tilde{\Psi}_{nk}\rangle. \quad (1)$$

The summation index i represents each atom species, each site position \vec{R} , and each of the partial wave components including all of their angular momentum quantum numbers (l, m) . The AE ϕ_i and PS $\tilde{\phi}_i$ partial waves are atomic functions which are designed to be equal outside the augmentation region, defined to be a sphere of radius r_c . Therefore, as in the NC (norm-conserving) scheme, $\Psi_n = \tilde{\Psi}_n$ outside a core radius (r_c). The projector functions \tilde{p}_i are dual to the PS partial waves:

$$\langle \tilde{p}_i | \tilde{\phi}_j \rangle = \delta_{ij}, \quad (2)$$

and are constructed to be confined within the augmentation region.

The PS wavefunctions $\tilde{\Psi}_{nk}$ are solutions of a generalized eigenvalue equation:

$$\tilde{H}\tilde{\Psi}_{nk} = \epsilon_{nk}O\tilde{\Psi}_{nk} \quad (3)$$

with

$$O = 1 + \sum_{ij} |\tilde{p}_i\rangle \langle (\phi_i | \phi_j) \rangle - \langle (\tilde{\phi}_i | \tilde{\phi}_j) \rangle \langle \tilde{p}_j| \quad (4)$$

and

$$\tilde{H} = -\frac{1}{2}\Delta + \tilde{v}_{\text{eff}} + \sum_{ij} |\tilde{p}_i\rangle D_{ij} \langle \tilde{p}_j|. \quad (5)$$

Here $\tilde{v}_{\text{eff}} = v_H[\tilde{n}_{Zc}] + v_H[\tilde{n} + \hat{n}] + v_{xc}[\tilde{n} + \tilde{n}_c]$ is an effective local potential and D_{ij} is a non-local term. v_H is the Hartree potential and v_{xc} the exchange–correlation potential. In the above equations, the quantities ϕ_i , $\tilde{\phi}_i$, \tilde{p}_i , \hat{n} , \tilde{n}_c , $v_H[\tilde{n}_{Zc}]$ are derived from atomic quantities that must be provided in the PAW atomic data file for each element. \tilde{n}_c is the pseudization of core electron charge density n_c . The contribution $v_H[\tilde{n}_{Zc}]$ represents the pseudization of Coulombic contributions from the nuclear charge Z and the core density.

2.1. All electron atomic calculations

As in other approaches, the first step in generating the PAW atomic data is to perform an AE calculation for a given atomic configuration. All wavefunctions (and projectors) are written as a product of radial and spherical harmonic functions:

$$\phi_i(\vec{r}) = \frac{\phi_{n_i l_i}(r)}{r} S_{l_i m_i}(\hat{r}) \quad (6)$$

with $S_{lm}(\hat{r})$ representing a real spherical harmonic function and with n_i indexing different partial waves for angular momentum l_i . It is assumed that the total electron density can be partitioned into a core electron density $n_c(r)$ corresponding to Q_{core} electrons and a valence electron density $n(r)$. The core density is assumed to be “frozen” in the same form in the solid as it is in the atom. The radial atomic eigenfunctions $\phi_{n_i l_i}$ are solution of:

$$[T + V_{\text{AE}}(r)]\phi_{n_i l_i}(r) = \epsilon_{n_i l_i} \phi_{n_i l_i}(r) \quad (7)$$

where T is the kinetic energy operator and $V_{\text{AE}}(r)$ is the self-consistent AE potential.

The AE partial wave basis functions $\phi_{n_i l_i}$ are solutions of the non-relativistic Schrödinger equation (Eq. (7)) or, for heavier elements, of the scalar-relativistic equation developed by Koelling and Harmon [22]. The transformation (1) implicitly supposes that the partial wave basis is complete. In practice, completeness is approximated by the choice of a finite number of partial wave basis functions, compromising accuracy and efficiency. Most of the time, a reasonable choice is to take two partial waves per angular momentum to perform simulations of materials in their ground state. To construct the AE basis set, the basis set energies $\epsilon_{n_i l_i}$ are first selected. The AE partial waves $\phi_{n_i l_i}$ are the corresponding solutions of Eq. (7). Often at least one of the AE partial waves $\phi_{n_i l_i}(r)$ is a bound state of the atom. In order to approximate the completeness criteria, unbound solutions of Eq. (7) are also used. The corresponding unbound partial wave functions $\phi_{n_i l_i}(r)$ need be evaluated only within the augmentation sphere.

2.2. Potential pseudization

The next step is to build a pseudopotential function $V_{\text{PS}}(r)$ that will be used to generate the PS partial waves $\tilde{\phi}_{n_i l_i}(r)$. In addition, the unscreened pseudopotential will be used to generate a local pseudopotential. In order to fulfill the requirements of the PAW formalism, $V_{\text{PS}}(r)$ is designed to smoothly match $V_{\text{AE}}(r)$ at a cutoff radius r_{loc} .

Several ways have been proposed in the literature to obtain V_{PS} [6,11,7]. The first possibility is to use the Troullier–Martins scheme originally formulated for norm-conserving pseudopotentials. [3]. We first choose a reference energy E_{loc} and a reference

angular momentum l_{loc} . A PS wavefunction is chosen to have the form

$$\phi_{PS}(r) = \begin{cases} r^{l_{loc}+1} \exp(p(r)) & \text{for } r \leq r_{loc} \\ \phi_{AE}(r) & \text{for } r > r_{loc}, \end{cases} \quad (8)$$

where $p(r)$ is an even 12th order polynomial. By design, ϕ_{PS} smoothly matches the corresponding AE wavefunction ϕ_{AE} at $r = r_{loc}$. The polynomial coefficients are determined from these matching conditions and other constraints including the norm-conservation condition $\int_0^{r_{loc}} |\phi_{PS}(r)|^2 r^2 dr = \int_0^{r_{loc}} |\phi_{AE}(r)|^2 r^2 dr$ [23]. From this choice of PS wavefunction, $V_{PS}(r)$ is determined by inverting the wave equation, which can be explicitly expressed in the form:

$$V_{PS}(r) = \begin{cases} E_{loc} + \frac{1}{2} \left\{ \frac{d^2 p}{dr^2} + \left(\frac{dp}{dr} \right)^2 + \frac{2(l_{loc} + 1)}{r} \frac{dp}{dr} \right\} & \text{for } r \leq r_{loc} \\ V_{AE}(r) & \text{for } r > r_{loc}. \end{cases} \quad (9)$$

A second possibility is to use an ultrasoft scheme without the norm conservation constraint. A PS wavefunction is chosen to have the form

$$\phi_{PS}(r) = \begin{cases} r^{l_{loc}+1} \sum_{m=0}^3 C_m r^{2m} & \text{for } r \leq r_{loc} \\ \phi_{AE}(r) & \text{for } r > r_{loc}. \end{cases} \quad (10)$$

As in the Troullier–Martins scheme, the polynomial coefficients C_m in the ultrasoft scheme are chosen so that $\phi_{PS}(r)$ is continuous and smooth particularly near $r = r_{loc}$. The corresponding pseudopotential $V_{PS}(r)$ is determined by inverting the wave equation for this choice of PS wavefunction; the resulting equation is similar to Eq. (9).

A third possible scheme [7] is to simply derive V_{PS} from V_{AE} by using a zero-order spherical Bessel function:

$$V_{PS}(r) = \begin{cases} \alpha \frac{\sin(qr)}{r} & \text{for } r \leq r_{loc} \\ V_{AE}(r) & \text{for } r > r_{loc}, \end{cases} \quad (11)$$

where the parameters α and q are chosen to ensure continuity of $V_{PS}(r)$.

For s or p elements, the Troullier–Martins norm-conserving scheme with $l_{loc} = l_{max} + 1$ (with l_{max} denoting the largest value of the angular momentum quantum number in the valence states) is often a good choice as it has good scattering properties. For d or f elements, this may lead to “ghost states” (unphysical states due to a numerical artifact, see [24]) and the second and third choices for $V_{PS}(r)$ may be preferable.

2.3. Wavefunction pseudization

2.3.1. The Vanderbilt scheme

In the formulation of US pseudopotentials [5,8], a scheme for generating PS partial waves and projectors was developed that can also be used for the PAW method. For each AE radial basis function $\phi_{n_i l_i}(r)$ a corresponding PS radial basis function $\tilde{\phi}_{n_i l_i}(r)$ is generated, designed to match smoothly at chosen radius $r_{n_i l_i}$. This pseudization can be performed in several ways. The form of the pseudized function can be either a polynomial:

$$\tilde{\phi}_{n_i l_i}(r) = r^{l_i+1} \sum_{m=0}^p C_m r^{2m} \quad (12)$$

or, following a RRKJ scheme [9], a sum of spherical Bessel functions:

$$\tilde{\phi}_{n_i l_i}(r) = \sum_{m=1}^p \alpha_m r_j^{l_i}(q_m r). \quad (13)$$

A slightly modified RRKJ scheme (modRRKJ) was recently introduced into the ATOMPAW code [25], designed to ensure that the corresponding projector functions have continuous first derivatives and to control the desired number of nodes in the pseudo basis functions [26]. The modRRKJ scheme needs further testing and has not been used in the current study.

For each smooth basis function, a localized auxiliary function can be formed:

$$|\chi_{n_i l_i}\rangle = (\epsilon_{n_i l_i} - T - V_{PS}) |\tilde{\phi}_{n_i l_i}\rangle \quad (14)$$

which by design vanishes for $r > r_c = \sup(r_{n_i l_i}, r_{loc})$. The projector functions are then formed from a linear combination of these auxiliary functions of the same angular momentum:

$$\tilde{p}_{n_j l_j}(r) = \sum_i \chi_{n_i l_i} (B^{-1})_{i,j} \delta_{i,l_j} \quad (15)$$

where the elements of the matrix B are given by:

$$B_{i,j} = \langle \tilde{\phi}_{n_i l_i} | \chi_{n_j l_j} \rangle. \quad (16)$$

As shown by Vanderbilt [5], this construction ensures that

$$\langle \tilde{\phi}_{n_i l_i} | \tilde{p}_{n_j l_j} \rangle = \delta_{ij} \quad (17)$$

and that the smooth function $\tilde{\phi}_{n_i l_i}(r)$ is an eigenfunction of the atomic PAW Hamiltonian.

2.3.2. The Blöchl scheme

In Blöchl's pseudofunction construction scheme [6], the projector functions are built with the help of a shape function $k(r)$ that vanishes outside the augmentation region. It can be for example:

$$k(r) = \begin{cases} \left[\frac{\sin(\pi r/r_c)}{(\pi r/r_c)} \right]^2 & \text{for } r < r_c \\ 0 & \text{for } r \geq r_c. \end{cases} \quad (18)$$

The pseudo basis functions $\tilde{\phi}_{n_i l_i}(r)$ are found by solving a self-consistent Schrödinger-like equation:

$$(T + V_{PS} - \epsilon_{n_i l_i}) |\tilde{\phi}_{n_i l_i}\rangle = C_{n_i l_i} k(r) |\tilde{\phi}_{n_i l_i}\rangle \quad (19)$$

with the constants $C_{n_i l_i}$ adjusted so that the logarithmic derivatives of $\phi_{n_i l_i}(r_c)$ and $\tilde{\phi}_{n_i l_i}(r_c)$ are equal. The corresponding projector functions are then formed according to:

$$\tilde{p}_{n_i l_i}(r) = \frac{k(r) \tilde{\phi}_{n_i l_i}(r)}{\langle \tilde{\phi}_{n_i l_i} | k | \tilde{\phi}_{n_i l_i} \rangle} \quad (20)$$

so that $\langle \tilde{p}_{n_i l_i} | \tilde{\phi}_{n_i l_i} \rangle = 1$. The final basis and projector functions $\phi_{n_i l_i}$, $\tilde{\phi}_{n_i l_i}$ and $\tilde{p}_{n_i l_i}$ are then obtained from the previous ones by a Gram–Schmidt orthogonalization procedure.

2.4. Core densities and unscreened potential

The last quantities that must be provided in the PAW atomic data file are n_c , \tilde{n}_c and $v_H[\tilde{n}_{Zc}]$. n_c is directly obtained from the AE calculation. It is then pseudized using a polynomial form inside a cut-off radius to obtain \tilde{n}_c . The case of $v_H[\tilde{n}_{Zc}]$ is more delicate. It is obtained by unscreening V_{PS} in such a way that the pseudopotential contributions from the atomic generation are consistent with the corresponding contributions in the treatment of solid materials. Two schemes are reported in the literature; the first scheme was developed by Blöchl [6] and a second scheme was developed by Kresse and Joubert [7]. Both schemes involve the use of a compensation charge density that is added to the pseudo charge density to ensure that each atom in both the atomic

calculation and within the periodic solid is represented with the correct multipole moments.

Besides requiring that the compensation charge be confined within the augmentation sphere, there are no restrictions on its shape. Several shapes for the radial component of compensation charge density $g_L(r)$ are in common use and are listed below. For the atomic system only the monopole ($L = 0$) moment is needed, but higher moments are needed in the solid state calculations. One choice is given by

$$g_L(r) = Nr^L k(r), \quad (21)$$

where $k(r)$ is the squared sinc function defined in Eq. (18). Another choice is a Gaussian shape function:

$$g_L(r) = Nr^L k(r) \quad \text{with } k(r) = \exp(-(r/d)^2). \quad (22)$$

Still another choice is a spherical Bessel function shape functions:

$$g_L(r) = \begin{cases} \sum_{i=1}^2 \alpha_{iL} (q_i r)^L & \text{for } r < r_c \\ 0 & \text{for } r \geq r_c. \end{cases} \quad (23)$$

In this case, the coefficients α_i and q_i are chosen so that the expression goes smoothly to 0 as r approaches r_c . In all of the cases, the shape functions are normalized so that when they are multiplied by the appropriate angular function, they integrate to unit multipole moment within the augmentation sphere. For $L = 0$, the integrated shape function satisfies $\int_0^{r_c} g_0(r) d^3r = 1$.

Blöchl's scheme [6] for pseudopotential generation makes use of a local pseudopotential function $\bar{v}(r)$ which is spacially localized within the augmentation radius and which is generated by descreening $V_{PS}(r)$ with corresponding atomic valence Hartree and exchange–correlation functions:

$$\bar{v} = V_{PS} - v_H[\tilde{n} + \tilde{n}_c + \hat{n}_B] - v_{xc}[\tilde{n} + \tilde{n}_c]. \quad (24)$$

Here \hat{n}_B is a compensation charge that is added to the pseudo charge density \tilde{n} to reproduce the correct multipole moments of the AE charge density including both core electron and nuclear charge contributions. Defining the Blöchl compensation charge in terms of one of the shape functions (Eqs. (21)–(23)) for the spherically symmetric ($L = 0$) function appropriate for the atomic case, it takes the form

$$\hat{n}_B(r) = g_0(r) \int_0^{r_c} [n(r') - \tilde{n}(r') + n_c(r') - \tilde{n}_c(r') + n_Z(r')] d^3r' \quad (25)$$

where $n_Z \equiv Z\delta(\mathbf{r}')$ represents the nuclear charge density. This analysis ensures that \bar{v} is a potential localized in the PAW sphere.

A second scheme is due to Kresse and Joubert [7] who define:

$$v_H[\tilde{n}_{Zc}] = V_{PS} - v_H[\tilde{n} + \hat{n}_K] - v_{xc}[\tilde{n} + \hat{n}_K + \tilde{n}_c] \quad (26)$$

where the Kresse–Joubert compensation charge density function \hat{n}_K depends only on the AE and PS valence electron density which expressed in terms of an $L = 0$ shape function takes the form.

$$\hat{n}_K(r) = g_0(r) \int_0^{r_c} [n(r') - \tilde{n}(r')] dr'. \quad (27)$$

The relationship between the two formulations can be written:

$$v_H[\tilde{n}_{Zc}] = \bar{v} + v_H[\tilde{n}_c + g_0(Q_{\text{core}} - \tilde{Q}_{\text{core}} - Z)] - v_{xc}[\tilde{n} + \hat{n}_K + \tilde{n}_c] + v_{xc}[\tilde{n} + \tilde{n}_c], \quad (28)$$

where $Q_{\text{core}} \equiv \int_0^{r_c} n_c(r) d^3r$ and $\tilde{Q}_{\text{core}} \equiv \int_0^{r_c} \tilde{n}_c(r) d^3r$. The main difference between the two treatments is the arrangement of the Coulombic contributions. While in the Blöchl formulation, \bar{v} is a localized pseudopotential, in the Kresse–Joubert formulation,

there is a long range Coulombic tail of the form $v_H[\tilde{n}_{Zc}] \rightarrow -(Z - Q_{\text{core}})/r$. Another contribution to the difference (Eq. (28)) is in the treatment of the exchange–correlation functions. There is no reason to include \hat{n}_K in the exchange–correlation term except for the convenience of storing the summed density function $\tilde{n} + \hat{n}$ rather than the quantities \tilde{n} and \hat{n} separately. In practice, the Kresse–Joubert formulation may lead to numerical error under certain conditions. For example, it has been shown that in the GGA approximation, when the shape of the compensation charge function is given by Eq. (21), the equilibrium lattice constant and the bulk modulus of Cu in the fcc structure are equal respectively to 0.367 nm and 120 GPa in the Blöchl formulation, whereas they are equal respectively to 0.374 nm and 110 GPa in the Kresse–Joubert formulation [16].

3. PAW atomic data generation

For each element, PAW atomic data generation follows the same steps as used to generate norm-conserving or US pseudopotentials. The first step is to choose the exchange–correlation functional (LDA-PW or GGA-PBE for instance) and to select the form of the wave equation (non-relativistic or scalar-relativistic).

3.1. Electronic configuration

The next step is the selection of the electronic configuration and the partitioning of the states into core and valence electron designations. The AE wavefunctions corresponding to valence states will be used in the construction of the partial wave basis, while the core states will be treated in the frozen core approximation. As a first approximation the valence states will be chosen from the outer shells of the configuration. However, in some cases it is necessary to include semi-core states in the set of valence electrons in order to simulate materials under special physical conditions, or to accurately represent transition metal or rare-earth materials. There are also some cases where physical conditions do not indicate a need for semi-core states, but the use of semi-core states provide mathematical stabilization by preventing the appearance of “ghost states” in the calculations [24, 23]. Rather than using the standard ground state configuration, it is sometimes useful to use an excited electronic configuration to generate a PAW dataset for the study of materials with significant charge transfer (such as oxides). However, in our experience, the results are not highly dependent on the chosen electronic configuration.

3.2. Choice of the grid and pseudization radii

It is recommended that a logarithmic grid is used for the AE atomic calculations in order that the differential equations can be accurately solved and the AE wavefunctions can be accurately represented in the region close to the nucleus. Indeed, it is very important, for instance, that the integral of the core electron density is consistent with the number of core electrons to high accuracy.

Pseudization cutoff radii for each valence orbital $\tilde{\phi}_{n_l i}$, for the screened pseudopotential V_{PS} , for core pseudodensity \tilde{n}_c , and for shape function g_0 are then chosen. The matching and cutoff radii must be chosen so that augmentation spheres do not overlap in the solid calculations. It is well-known that the choice of radii is crucial for the efficiency of the PAW atomic data. A compromise must be found between the use of small radii, which will generally result in better numerical accuracy but needs a large plane wave energy cutoff, and the use of larger radii, which may produce results with worse numerical accuracy but converges with a smaller plane wave

energy cutoff. Another tool to reduce the energy cutoff is to use Fourier filtering, as proposed for instance in [27], but we have not used it in this study.

3.3. Generation of the partial wave basis

The partial wave basis is composed of the valence electron states and, if necessary for accuracy, supplementary partial waves $\phi_{n_l l_i}$ with the choice of corresponding reference energies $\epsilon_{n_l l_i}$. We have generally chosen to have 2 partial-waves per angular momentum in the basis. (This choice is not necessarily optimal, but adequate in most cases.) When we need to calculate a great number of bands above the Fermi level (DFT conductivity calculations for instance) it may be necessary to add a third partial-wave per angular momentum with a higher (positive) energy reference to improve the completeness of the partial wave basis and to better represent wavefunctions states above the Fermi level.

The pseudization scheme for wavefunctions is then chosen (Blöchl, Vanderbilt polynomial or RRKJ). We have noticed that Blöchl scheme for generating projectors and pseudo basis functions can produce very accurate datasets but sometimes the resulting calculations on periodic solids have a low efficiency (in the sense that they may need a large number of plane waves to converge the DFT calculation). It is our experience that the Vanderbilt scheme results in a significantly more efficient calculation. It is our experience that for most cases, the best performance is obtained using the RRKJ scheme.

From the PAW atomic calculation itself there is some important information about the accuracy of PAW atomic data. For example, it is recommended that the functions $\phi_{n_l l_i}(r)$, $\tilde{\phi}_{n_l l_i}(r)$ and $\tilde{p}_{n_l l_i}(r)$ all have comparable magnitudes to avoid numerical instability and to promote a good transferability. If this is not the case, several options are possible.

- Adjust the matching and cutoff radii (without allowing overlapping spheres in the solid calculations).
- Change the pseudopotential scheme.
- Adjust the reference energies for unbound partial wave basis functions or additional basis functions. Changing the reference energy can reduce the magnitude of projectors, but it is important to check that the logarithmic derivatives are correct [23] as will be discussed further below.

To have accurate representation properties, for each l -quantum number included in the partial wave basis, PAW atomic data must lead to logarithmic derivatives of the eigenfunctions of the PAW atomic Hamiltonian that match the corresponding logarithmic derivatives of the eigenfunctions of the AE atomic Hamiltonian. By construction, the logarithmic derivatives are equal at the energies of the basis functions. If the agreement is not good enough, the reference energy for unbound states can be changed. Discontinuities in the logarithmic derivatives of the AE partial wavefunctions represent the energies at which the wavefunctions have a node at the matching radius. A reasonable choice of an unbound reference energy avoids these node energies. However if a unbound reference energy is too close to the energy of other basis functions, the basis set is unable to span the function space required for accurate calculations in the solid. This is often reflected in the form of the projector functions. Each projector being a dual function of one wavefunction, it must obey simultaneously to a constraint of normalization for one wavefunction and to a constraint of orthogonalization for the other wavefunction. If the basis functions are too close in shape, the projector functions may have a large amplitude compared to the amplitude of the wavefunctions and this may lead to numerical instabilities. In addition, a poor choice of basis functions can be reflected in the poor agreement between the logarithmic derivatives of the AE and PS calculations in some of the energy

range of interest. Another possible problem is the appearance of a discontinuity in the PAW logarithmic derivative curve at an energy where the exact logarithmic derivative is continuous. Most of the time, this shows the presence of a “ghost state”. It is sometimes possible to change the values of the reference energies in order to make the ghost state disappear. Alternatively, adjusting the method of pseudization V_{AE} can also help avoid ghost states.

3.4. Pseudization of the local potential

As already seen above, the pseudization scheme for the local potential can be chosen among Troullier–Martins, ultrasoft, or Bessel schemes. Norm-conserving pseudopotentials are sometimes so deep (attractive near $r = 0$) that they produce “ghost states”. To eliminate a ghost state [23], one may select a different angular momentum quantum number l_{loc} and adjust the matching radius r_{loc} . Another solution is to change the pseudopotential scheme. Selecting a simple Bessel pseudopotential (Eq. (11)) or ultrasoft pseudopotential (Eq. (10)) often avoids ghost state solutions. However, it is our experience, that in order to obtain accurate results in solid calculations, it is often necessary to reduce the matching radius r_{loc} . Denoting the largest matching radius as r_{PAW} , we find that it is often reasonable to choose $0.6 r_{PAW} \leq r_{loc} \leq 0.8 r_{PAW}$. A convenient way to find the best choice for r_{loc} is to check the valence energies obtained from a PAW atomic calculation compared to a reference atomic all-electron (AE) calculation. By adjusting r_{loc} , the agreement can be improved.

4. PAW atomic data validation and efficiency

4.1. PAW atomic data validation

The PAW method is an all-electron method that uses auxiliary functions (plane waves for instance) as working functions. If the basis of partial waves is complete, PAW results must be in agreement with reference all electron calculations. The question of the measurement of the agreement of PAW and AE calculation is still a subject of debate. Most of the time, a solid state calculation is performed and the equilibrium volumes and bulk moduli are compared. This can be done for several environments, such as for metals or oxides, as has been recently studied for the GBRV potentials [19].

To have a more flexible tool that allows comparisons between codes and between PAW atomic data tables, Lejaeghere et al. have recently introduced a new measure, named Δ , of the agreement between two codes for a given structure [17]. It is defined as the difference between the two equations of state, obtained by the two codes:

$$\Delta = \sqrt{\frac{\int \Delta E^2(V) dV}{\Delta V}}. \quad (29)$$

In this equation, $\int \Delta E^2(V) dV = \int_{V_i}^{V_f} (E_{code1}(V) - E_{code2}(V))^2 dV$ and $\Delta V = V_f - V_i$. The integrals over the initial and final volumes of the structure are illustrated as the shaded region in Fig. 1. From the use of Eq. (29) to determine the value of Δ for each element, a mean value for all of the elements in the dataset can be determined. This Δ assessment measure has been obtained for several codes and several pseudopotential and is reported on the web site of the authors [28]. The web site also provides the downloadable delta calculation package which includes the results of solid state calculations for 71 elements obtained with the AE code Wien2k [29] (the equilibrium volume V_{AE} , the bulk modulus B_{AE} and its derivative B'_{AE}), as well as the associated crystallographic data.

We have used the delta calculation package to validate our code and our new atomic data in comparison with the Wien2k

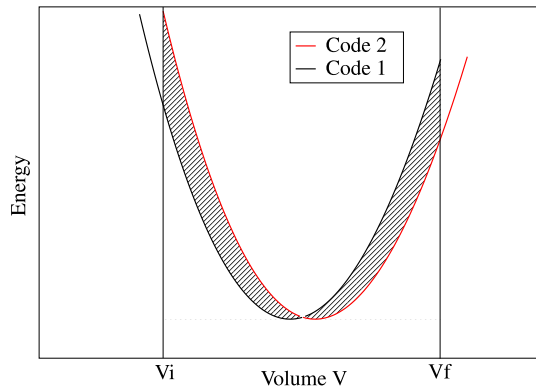


Fig. 1. A schematic comparison of the equations of state (EOS) obtained by two codes: Code 1 (black) and Code 2 (red), with the difference area over some volume interval $[V_i, V_f]$ indicated by shading. (For interpretation of the references to colour in this figure legend, the reader is referred to the web version of this article.)

code. The electronic structure calculations for the 71 elements have been performed using the ABINIT code [14]. We have used the recommended values [17] for the k-point sampling (6750/N k-points in the Brillouin zone for a N-atom cell). A Fermi-Dirac broadening of 0.002 Ha has been used to approximate the Brillouin zone integrals. As indicated in [17], we have used the crystallographic data (CIF files) provided with the delta calculation package. In order to perform the test calculations with exactly the same conditions as Wien2k comparison data, the total energy of each element was evaluated at seven different volumes, without geometry optimization of the internal parameters, ranging from 0.94 to 1.06 V_S , where V_S is the equilibrium volume deduced from the CIF file. For each element, the results for $E_{Abinit}(V)$ were fit to the Birch–Murnaghan Equation of State (EOS) to obtain values V_0 (equilibrium volume), B (bulk modulus) and B' (the derivative the bulk modulus) which could be compared with the corresponding AE values V_{AE} , B_{AE} , and B'_{AE} .

The first step has been to validate the ABINIT code against the Delta calculation process. For this we have used the PAW atomic data labeled “PAW 0.9” provided on the GPAW web site [18]. In order to implement the use of GPAW datasets within ABINIT, two modifications to the ABINIT code were made. First since the GPAW atomic data are provided in a XML format, we have implemented the reading of XML files in ABINIT. Secondly, we added to ABINIT the capability of using the same radial grid used in the PAW 0.9 package which is given for n grid points with index i ($0 \leq i \leq n - 1$) by $r(i) = \frac{a \cdot i}{n - i}$. We performed the ABINIT calculation for the 68 elements of the PAW 0.9 table, obtaining a mean value of $\Delta = 1.6$ meV for both a cutoff energy of 20 Ha and 40 Ha. This value is very close to the value obtained directly with the GPAW code with the same PAW 0.9 package (1.7 meV) [28]. The small value of Δ obtained using ABINIT validates the accuracy of the ABINIT code in comparison with similar codes and the Delta calculation process.

4.2. PAW atomic data table generation

The second step has been to generate a new PAW atomic data table following the methodology described above in Sections 2 and 3. We have generated a table of 71 PAW atomic data corresponding to elements ranging from H to Rn, without At and lanthanides (except Lu). All the PAW data have been obtained using the ATOMPAW generator (v3.1.0.2) [25], starting either from existing input files already provided on the ABINIT web site [30], or from new input files. All the schemes discussed in Section 2 are implemented in ATOMPAW, which makes it a very flexible tool.

With respect to the choice of the electronic configurations, from H to Be, all the electrons are taken as valence electrons. For columns

IA, IIA, IIIB to VIIIB of the periodic table of elements, s and p semi-core states are included in the valence. For columns IB and IIB, only s and d electrons are taken as valence electrons. For columns IIIA to VIIIA, only s and p electrons are taken as valence electrons. For Lu, the f electrons are also included in the valence electrons. For Pt, only s and d electrons are taken as valence electrons.

For the radial grid, a logarithmic grid was used with the form $r(i) = a(\exp(d \cdot (i - 1)) - 1)$, where $1 \leq i \leq n$. The partial wave basis included at least 2 partial waves per angular momentum. The PAW atomic dataset was designed to be well converged when used with a plane wave energy cutoff of 20 Ha in the ABINIT code and the cutoff radii were chosen accordingly. For this, we have tested each element in the ABINIT code with a cutoff energy of 12, 15, 20, and 40 Ha for plane waves. If a test PAW atomic dataset did not converge with the 20 Ha cutoff, the cut-off radii were increased until the convergence was achieved. All the calculations were performed with the GGA-PBE exchange and correlation functional in a scalar-relativistic framework. The crystallographic structures used for each element is described in [17].

We obtain a mean value of $\Delta = 0.4$ meV for our whole table (named JTH table). The values of Δ for each element are shown in Fig. 2. The use of the Δ factor is very convenient: it allows for a global measure of the accuracy of atomic data for each element, as well as a mean value that characterizes a whole atomic dataset. The value of 0.4 meV is very good compared with values already published for other codes or for other PAW atomic data packages, where the smallest values of Δ are in the range 1.6–1.8 meV [28,17].

However, one must be aware of some drawbacks using the Δ factor.

- The Δ value is by construction very dependent on the AE calculations that are used for comparison. This means that we must be very confident in the AE results, which may be difficult to obtain. It is certainly necessary that the AE community agrees on the tuning of the AE codes so that the values of V_{AE} (the equilibrium volume), B_{AE} (the bulk modulus) and B'_{AE} (the derivative of the bulk modulus) are well established for each element in the studied crystallographic structures. It would also be useful to add lanthanides and actinides in the AE references.
- The Δ factor is based on calculations on pure elements in their ground state crystallographic structures. It is also interesting to have comparison with AE calculations in compounds like oxides, as has been already done on the ATOMPAW web site [26] and by Garrity et al. [19].
- In view of high-throughput calculations, it is extremely important to have efficient PAW atomic data. The Δ factor must therefore be given with an energy cut-off, and its convergence with the energy cut-off must be given.
- What is the accuracy of the Δ factor? What does it means to have $\Delta = 0.2$ meV rather than 0.5 meV?
- We have noticed that for some elements, the Δ factor is very sensitive to the values V_0 , B and B' obtained as a result of the tuning of the input parameters of the atomic data generator. This is not the case at all for other elements.

We therefore propose in the next section an alternative definition of a Δ factor to account for some of these drawbacks.

4.3. PAW atomic data efficiency: towards a new Δ factor definition

The reason why some elements are very sensitive to the accuracy of V_0 , B and B' (compared to the AE values) comes from the large variation of the V_0 and B values over the elements. V_0 indeed ranges from 7.2 Bohr³ for Boron to 117.7 Bohr³ for Cs, whereas B ranges from 0.57 GPa for Ar to 401 GPa for Os, nearly three order of magnitude. This means that a very small deviation of V_0 from the

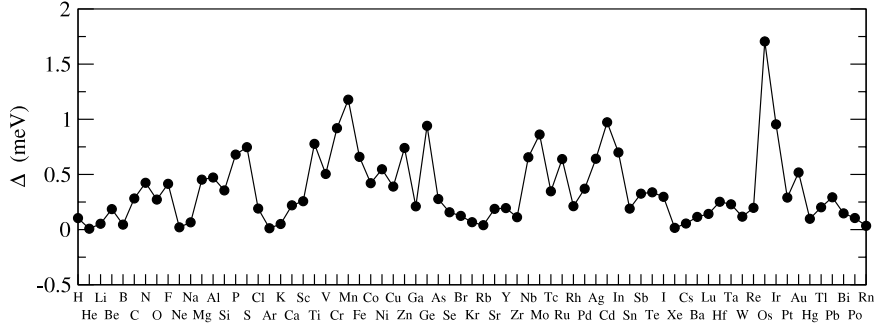


Fig. 2. Δ value as a function of element for a 20 Ha energy cut-off for the JTH table.

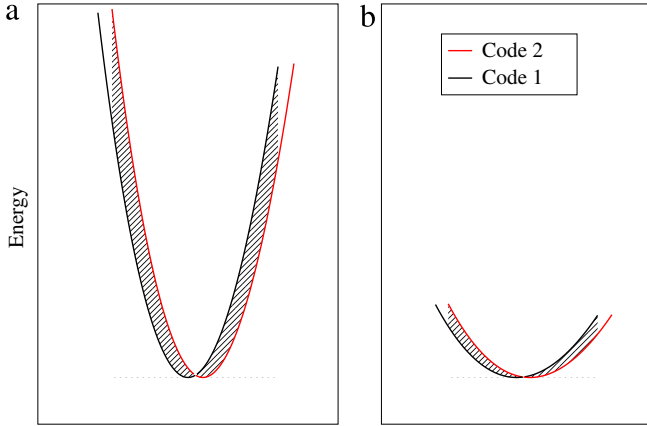


Fig. 3. Comparison of the EOS obtained by two codes (a) for a high value of the bulk modulus (b) for a small value of the bulk modulus.

reference AE value will give a very large value of the Δ factor for a large B value (Fig. 3(a)), whereas a large deviation of V_0 from the reference AE value will give a very small value of the Δ factor for a small B value (Fig. 3(b)).

For instance, using ABINIT with the PAW 0.9 atomic data, we find a V_0 deviation of 0.76% for Cs leads to $\Delta_{Cs} = 0.39$ meV whereas a V_0 deviation of 0.76% for Os leads to $\Delta_{Os} = 9.14$ meV. The same effect happens between elements that have close bulk moduli but large differences in their equilibrium volumes.

To overcome this difficulty, we propose to define a Δ_1 factor, which is similar to the original Δ factor except it is “renormalized” to reference values of V_0 and B for all the elements. Indeed the Birch–Murnaghan energy is directly proportional to V_0 and B (see Appendix), and so is the Δ factor (to first order). For each element, we therefore define:

$$\Delta_1 = \frac{V_{ref} B_{ref}}{V_{AE} B_{AE}} \Delta. \quad (30)$$

The Δ_1 factor is a re-scaled value of Δ to a reference material characterized by an equilibrium volume V_{ref} and a bulk modulus B_{ref} . This allows a comparison of the Δ_1 factor of all the elements, as it is normalized to the same reference. We have chosen the values of $V_{ref} = 30 \text{ Bohr}^3$ and $B_{ref} = 100 \text{ GPa}$ as they correspond approximatively to the mean values of V_0 and B over the 71 elements tested.

We have then calculated the Δ and Δ_1 factor for four energy cut-offs (12 Ha, 15 Ha, 20 Ha, 40 Ha) and the atomic datasets available with the ABINIT code: the GPAW PAW 0.9 package, the GBRV-v1 package [31], and our new package (named JTH). A fourth package is under construction by the PWPAAW group [26] but the work is in progress and we have not used this package in this paper. The results are presented in Tables 1 and 2.

Table 1

Comparison of the Δ values (meV) as a function of cut-off energy for three PAW atomic datasets, as calculated with the ABINIT code.

Δ (meV)	12 Ha	15 Ha	20 Ha	40 Ha
JTH (71 elements)	2.461	0.817	0.363	0.453
PAW 0.9 (68 elements)	4.845	2.289	1.559	1.552
GBRV-v1 (63 elements)	4.486	2.617	2.420	2.345

Table 2

Comparison of the Δ_1 values (meV) as a function of cut-off energy for three PAW atomic datasets, as calculated with the ABINIT code.

Δ_1 (meV)	12 Ha	15 Ha	20 Ha	40 Ha
JTH (71 elements)	7.671	2.187	0.888	0.970
PAW 0.9 (68 elements)	12.117	5.267	3.092	2.828
GBRV-v1 (63 elements)	8.243	5.698	5.363	5.155

For further comparison, when using the values given in [17] for the VASP package (71 elements) [7], we obtain $\Delta = 1.920$ meV and $\Delta_1 = 3.786$ meV (As indicated in [17], the energy cutoff is 15 Ha for most elements and 22 Ha for He, B, C, N, O, F and Ne). For the three packages (JTH, PAW 0.9, GBRV-v1), Δ and Δ_1 are well converged for a 20 Ha energy cutoff. For all the energy cutoffs, the JTH package gives smaller Δ and Δ_1 values than the other two. For Δ , the difference is around 1.2 meV whereas for Δ_1 the difference is around 2 meV for converged energy cutoffs, between the JTH table and the PAW 0.9 table.

If we look in detail at the Δ factor (Fig. 4), we can see that for the GBRV-v1 package, only two elements (N, O) are above 10 meV. Without these two elements, $\Delta = 1.484$ meV, which is a very good result when compared to the other packages [32].

With respect to Δ_1 , (Fig. 5), the same trends are found: omitting the elements H, N, O for which $\Delta_1 > 20$ meV, $\Delta_1 = 2.944$ meV for the GBRV-v1 package. The Δ_1 factor, treating low and high equilibrium volume and bulk modulus elements on an equal footing, allows an easy identification of questionable elements for which the Δ_1 is very high compared to the mean Δ_1 . It is also noticeable that the JTH package has quite low values of Δ and Δ_1 for a 15 Ha energy cutoff, which is essential in the framework of high-throughput calculations.

5. Conclusions

Thanks to the flexibility of the ATOMPAW generator, we have been able to generate a 71 element PAW dataset table. This JTH table has been validated against AE calculations using the Δ factor and also the modified Δ_1 factor we have defined in this paper. The JTH table has good accuracy and efficiency compared to other packages which makes it a good candidate for high-throughput calculations. This new table is provided in the XML format, that makes it easily readable by all the PAW codes. It is distributed on the ABINIT web site [30].

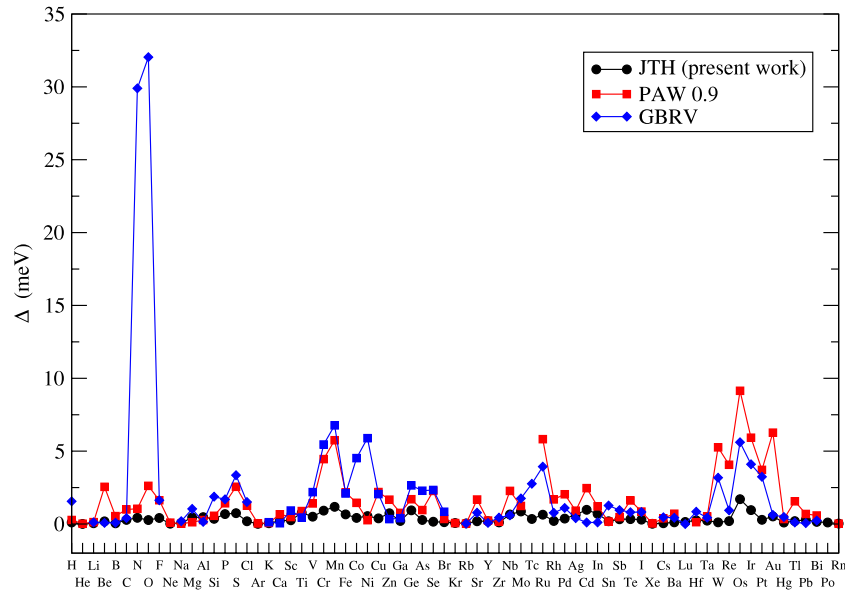


Fig. 4. Δ value as a function of element for a 20 Ha energy cut-off: comparison between JTH, PAW 0.9 and GBRV.

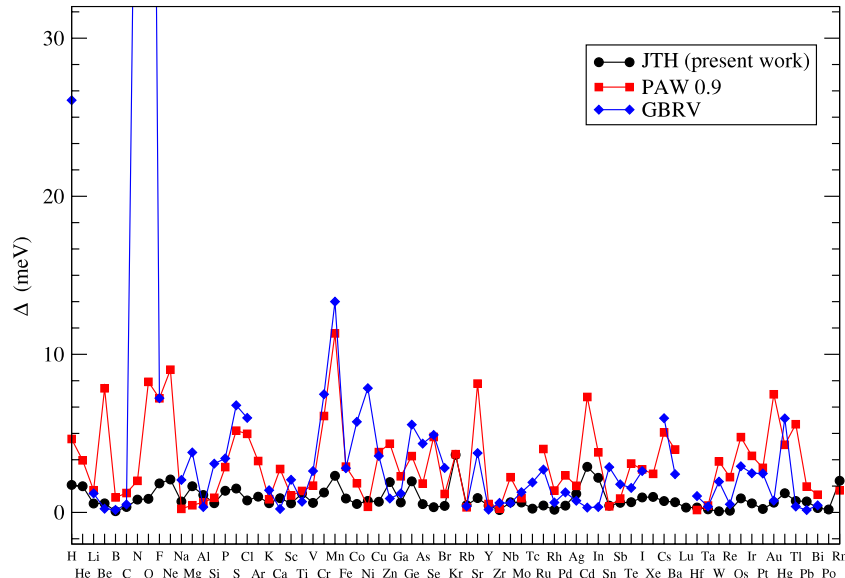


Fig. 5. Δ_1 value as a function of element for a 20 Ha energy cut-off: comparison between JTH, PAW 0.9 and GBRV.

Acknowledgments

The authors thank Bernard Amadon and Kevin Garrity for helpful discussions concerning the generation of PAW atomic data. This work was partly performed using HPC resources from the French Research and Technology Computing Center (CCRT). The contributions by NH to this effort was supported by NSF Grant No. DMR-1105485.

Appendix. The Birch–Murnaghan energy

$$E(V) - E_0 = \frac{9V_0B}{16} \left[\left(\frac{V_0}{V} \right)^{2/3} - 1 \right]^3 B' + \left[\left(\frac{V_0}{V} \right)^{2/3} - 1 \right]^2 \left[6 - 4 \left(\frac{V_0}{V} \right)^{2/3} \right] \quad (A.1)$$

is proportional to B , so that obviously, the Δ factor also: if one element A has a bulk modulus $B_A = \alpha B_C$, where C is another element, $\Delta_B \simeq \alpha \Delta_C$, with the hypothesis that $B_A^{code1} = \alpha B_C^{code1}$ and $B_A^{code2} \simeq \alpha B_C^{code2}$.

This is the same thing for the dependence against V_0 , although it is more tedious to establish:

Let us consider 2 elements A and C and suppose that $V_0^{code1}(A) = \alpha V_0^{code1}(C)$ and $V_0^{code2}(A) = \alpha V_0^{code2}(C)$ for simplicity (with the same B and B' for the two elements). The segment in which Δ is computed is defined by $V_i = 0.94V_S$ and $V_f = 1.06V_S$ where V_S is the center of the segment. V_S is close to V_0^{code1} and V_0^{code2} , and for simplicity, we suppose that $V_S(A) \simeq V_S(C)$.

As shown in the Appendix of [17],

$$\Delta = \sqrt{\frac{F(V_f) - F(V_i)}{V_f - V_i}} \quad (A.2)$$

where

$$F(V) = \int_{V_i}^{V_f} (E_{code1}(V) - E_{code2}(V))^2 dV = \sum_{n=-2}^4 x_n V^{-(2n+1)/3} \quad (\text{A.3})$$

using the definition of x_n given in [17].

It can then be shown that each of the seven terms contributing to F is proportional to α^3 . For instance, for $n = 4$, the contribution to $F_A(V_f)$ is:

$$\begin{aligned} & x_4^A (V_f^A)^{-3} \\ &= -\frac{1}{3} \left(\frac{9(V_0^{code1}(A))^3 B_A^{code1}}{16} (B'_{code1}(A) - 4) \right. \\ & \quad \left. - \frac{9(V_0^{code2}(A))^3 B_A^{code2}}{16} (B'_{code2}(A) - 4) \right)^2 (1.06V_S(A))^{-3} \\ &\simeq -\frac{\alpha^6}{3} \left(\frac{9(V_0^{code1}(C))^3 B_C^{code1}}{16} (B'_{code1}(C) - 4) \right. \\ & \quad \left. - \frac{9(V_0^{code2}(C))^3 B_C^{code2}}{16} (B'_{code2}(C) - 4) \right)^2 (1.06\alpha V_S(C))^{-3} \\ &\simeq \alpha^3 x_4^C (V_f^C)^{-3}. \end{aligned} \quad (\text{A.4})$$

We have therefore $F_A(V_f) \simeq \alpha^3 F_C(V_f)$, $F_A(V_i) \simeq \alpha^3 F_C(V_i)$ and $V_f^A - V_i^A \simeq \alpha(V_f^C - V_i^C)$.

So, at the end:

$$\Delta(A) \simeq \alpha \Delta(C). \quad (\text{A.5})$$

References

- [1] D. Hamann, M. Schlüter, C. Chiang, Norm-conserving pseudopotentials, *Phys. Rev. Lett.* 43 (1979) 1494.
- [2] L. Kleinman, D. Bylander, *Phys. Rev. Lett.* 48 (1982) 1425.
- [3] N. Troullier, J.L. Martins, *Phys. Rev. B* 43 (1991) 1993.
- [4] S. Goedecker, M. Teter, J. Hutter, Separable dual-space gaussian pseudopotentials, *Phys. Rev. B* 54 (1996) 1703.
- [5] D. Vanderbilt, Soft self-consistent pseudopotentials in a generalized eigenvalue formalism, *Phys. Rev. B* 41 (1990) 7892.
- [6] P. Blöchl, Projector augmented-wave method, *Phys. Rev. B* 50 (1994) 17953.
- [7] G. Kresse, D. Joubert, From ultrasoft pseudopotentials to the projector augmented-wave method, *Phys. Rev. B* 59 (1999) 1758.
- [8] K. Laasonen, A. Pasquarello, R. Car, C. Lee, D. Vanderbilt, Car–Parrinello molecular dynamics with Vanderbilt ultrasoft pseudopotentials, *Phys. Rev. B* 47 (1993) 10142.
- [9] A.M. Rappe, K.M. Rabe, E. Kaxiras, J.D. Joannopoulos, *Phys. Rev. B* 41 (1990) 1227.
- [10] J. Furthmüller, P. Käckel, F. Bechstedt, G. Kresse, Extreme softening of Vanderbilt pseudopotentials: General rules and case studies of first-row and d-electron elements, *Phys. Rev. B* 61 (2000) 4576.
- [11] A. Tackett, N. Holzwarth, G. Matthews, A projector augmented wave (paw) code for electronic structure calculations, part ii: pwpaw for periodic solids in a plane wave basis, *Comput. Phys. Comm.* 135 (2001) 348.
- [12] G. Kresse, J. Furthmüller, *Comput. Mater. Sci.* 6 (1996) 15.
- [13] J. Mortensen, L. Hansen, K. Jacobsen, A real-space grid implementation of the projector augmented wave method, *Phys. Rev. B* 135 (2001) 348.
- [14] X. Gonze, B. Amadon, P.-M. Anglade, J.-M. Beuken, F. Bottin, P. Boulanger, F. Bruneval, D. Caliste, R. Caracas, M. Cote, T. Deutsch, L. Genovese, P. Ghosez, M. Giantomassi, S. Goedecker, D.-R. Hamann, P. Hermet, F. Jollet, G. Jomard, S. Leroux, M. Mancini, S. Mazevet, M. Oliveira, G. Onida, Y. Pouillon, T. Rangel, G.-M. Rignanese, D. Sangalli, R. Shaltaf, M. Torrent, M. Verstaete, G. Zerah, J. Zwanziger, Abinit: first-principles approaches to material and nanosystem properties, *Comput. Phys. Comm.* 180 (2009) 2582–2615.
- [15] P. Giannozzi, S. Baroni, N. Bonini, M. Calandra, R. Car, C. Cavazzoni, D. Ceresoli, G.L. Chiarotti, M. Cococcioni, I. Dabo, A.D. Corso, S. Fabris, G. Fratesi, S. de Gironcoli, R. Gebauer, U. Gerstmann, C. Gougousis, A. Kokalj, M. Lazzeri, L. Martin-Samos, N. Marzari, F. Mauri, R. Mazzarello, S. Paolini, A. Pasquarello, L. Paulatto, S. Sbraccia, S. Scandolo, G. Sclauzero, A.P. Seitsonen, A. Smogunov, P. Umari, R.M. Wentzcovitch, Quantum espresso: a modular and open-source software project for quantum simulations of materials, *J. Phys.: Condens. Matter* 21 (2009) 395502.
- [16] M. Torrent, N. Holzwarth, F. Jollet, D. Harris, N. Lepley, X. Xu, Electronic structure packages: Two implementations of the projector augmented-wave method (paw) formalism, *Comput. Phys. Comm.* 181 (2010) 1862–1867.
- [17] K. Lejaeghere, V. Van Speybroeck, G. Van Oost, S. Cottenier, Error estimates for solid-state density-functional theory predictions: an overview by means of the ground-state elemental crystals, *Crit. Rev. Solid State Mater. Sci.* 39 (2014) 1.
- [18] <http://wiki.fysik.dtu.dk/gpaw/setups>, 2013.
- [19] K.F. Garrity, J.W. Bennett, K.M. Rabe, D. Vanderbilt, Pseudopotentials for high-throughput DFT calculations, *Comput. Mater. Sci.* 81 (2014) 446–452.
- [20] N. Holzwarth, G. Matthews, R. Dunning, A. Tackett, Y. Zeng, Comparison of the projector augmented-wave, pseudopotential, and linearized augmented-plane-wave formalisms for density-functional calculations of solids, *Phys. Rev. B* 55 (1997) 2005.
- [21] M. Torrent, F. Jollet, F. Bottin, G. Zerah, X. Gonze, Implementation of the projector augmented-wave method in the Abinit code, *Comput. Mater. Sci.* 42 (2008) 337–351.
- [22] D.D. Koelling, B.N. Harmon, A technique for relativistic spin-polarised calculations, *J. Phys. C: Solid State Phys.* 10 (1977) 3107.
- [23] M. Fuchs, M. Scheffler, Ab initio pseudopotentials for electronic structure calculations of poly-atomic systems using density-functional theory, *Comput. Phys. Comm.* 119 (1999) 67.
- [24] X. Gonze, P. Käckel, M. Scheffler, Ghost states for separable, norm-conserving, ab initio pseudopotentials, *Phys. Rev. B* 41 (1990) 12264.
- [25] N. Holzwarth, A. Tackett, G. Matthews, A projector augmented wave (paw) code for electronic structure calculations, part i: atompaw for generating atom-centered functions, *Comput. Phys. Comm.* 135 (2001) 329.
- [26] <http://users.wfu.edu/natalie/papers/pwpaw/newperiodictable/>, 2013.
- [27] R.D. King-Smith, M.C. Payne, J.S. Lin, Real-space implementation of nonlocal pseudopotentials for first-principles total-energy calculations, *Phys. Rev. B* 44 (1991) 13063.
- [28] Comparing solid state DFT codes, basis sets and potentials, 2013, <http://molmod.ugent.be/DeltaCodesDFT>.
- [29] P. Blaha, K. Schwarz, G. Madsen, D. Kvasnicka, J. Luitz, WIEN2k, An Augmented Plane Wave + Local Orbitals Program for Calculating Crystal Properties (Karlheinz Schwarz, Techn. Universität Wien, Austria), 2001. ISBN 3-9501031-1-2, <http://www.wien2k.at>.
- [30] <http://abinit.org>, 2013.
- [31] For the GBRV-v1 table with 12 Ha cutoff, Ni has been omitted for the calculation of the delta factor as it has not been possible to obtain a converged ferromagnetic phase, 2013.
- [32] These values have been greatly improved with the v1.01 version of the GBRV table for which $\Delta_0 = 3.330$ meV and $\Delta_N = 7.279$ meV which leads to a mean value of $\Delta = 1.606$ meV for the whole table, 2013.